

Transonic airfoil buffet at high Reynolds number by using wall-modeled large-eddy simulation

Yuma Fukushima

Department of Aerospace Engineering
Tohoku University
6-6-01 Aramaki-Aza-Aoba, Aoba-ku, Sendai
980-8579, JAPAN
Email : fukushima@cfm.mech.tohoku.ac.jp

Soshi Kawai

Department of Aerospace Engineering
Tohoku University
6-6-01 Aramaki-Aza-Aoba, Aoba-ku, Sendai
980-8579, JAPAN
Email : kawai@cfm.mech.tohoku.ac.jp

ABSTRACT

In this study, a wall-modeled large-eddy simulation (WMLES) of transonic buffet phenomena over an OAT15A supercritical airfoil at high Reynolds number is conducted. By using the WMLES, the buffet onset is successfully predicted. The small separation near a trailing edge is also accurately estimated with buffet phenomena. The flow physics of buffet flow are investigated from the results. As a results, it is confirmed that there are dominant phenomena in low and high frequency band. By using the phase average operation, large-scale vortical structures with low frequency band and acoustic waves generated from the trailing edge are identified. At last, we propose the new self-sustained oscillation model which depends on the pressure ratio forward and backward of the shock wave. The possibility of the proposed model is confirmed from the results.

INTRODUCTION

Transonic buffet is one of the famous unsteady phenomena related to the flying aircraft. Buffet phenomena involve the vibration related to weak flow separation after the shock wave on an airfoil and affect the comfort and safeness of the aircrafts' operation. For the computational investigation, LES is suitable for such kind of unsteady flow including the separation. However, the turbulent boundary layer at high Reynolds number induces the unreachable computational cost in the wall-resolved LES. Choi and Moin estimated the required number of grid points for the wall-resolved LES as $N_{total} = Re_c^{13/7}$ (Choi and Moin, 2012). To avoid the large computational cost, methods of modelling the inner-layer turbulence are proposed instead of resolving the turbulence in the inner-layer.

One category of modelling the inner-layer wall turbulence is a wall-stress-models (see recent review of Larsson et al., 2016). This kind of model is mainly based on the momentum conservation in a parallel shear flow. In the wall-modeled LES (WMLES), only the inner-layer of the boundary layer is modeled, and the outer-layer is computed by LES. Kawai and Larsson pointed out the numerical and subgrid modelling errors derived from the LES computation near the wall and proposed the simple solution to bypass this errors in the WMLES computation (Kawai and Larsson, 2012). This model was extended to the flow without equilibrium assumption and applied to a shock/boundary-layer interaction problem (Kawai and Larsson, 2013) and a separated flow over an airfoil near stall condition at high Reynolds number (Kawai and Asada, 2013). From the results, it is considered that the wall-models have potential to predict the buffet phenomena involving shock wave and turbulent boundary layer interactions.

In this study, the proposed WMLES is applied to the transonic buffet simulation around the OAT15A to investigate the applicability of the WMLES. Buffet flow conditions are $Re_c = 3.0 \times 10^6$, $\alpha = 3.5deg$, and $M_\infty = 0.73$. For comparison, non-buffet condition ($Re_c = 3.0 \times 10^6$, $\alpha = 3.5deg$, and $M_\infty = 0.715$) is also computed. Computational results are compared with the experimental data and

the results by Deck (2005). To understand the buffet phenomena in detail, the flow physics and acoustic waves generated from the trailing edge (Hartmann et al., 2013) are investigated and discussed. At last, a new self-sustained oscillation mechanism is proposed and investigated from the obtained results.

NUMERICAL METHODS

The compressible spatially-filtered Navier-Stokes equations are solved in the LES mesh that is generated to resolve the outer-layer turbulence with modeled shear stresses and heat fluxes at the wall. The spatial derivatives are evaluated by the sixth-order compact differencing scheme (Lele, 1992) with an eight-order low-pass filter (Gaitonde and Visbal, 2000). The third-order total variation diminishing Runge-Kutta scheme (Gottlieb and Shu, 1998) is used for time integration. The localized artificial diffusivity method is used to robustly capture the shock waves (Kawai et al., 2010). A selective mixed-scale model (Lenormand et al., 2000) is used to calculate the sub-grid scale turbulent eddy viscosity μ_t and turbulent Prandtl number $Pr_t = 0.9$. The wall model with equilibrium assumption (Kawai and Larsson, 2012) solves the equilibrium boundary layer equations in an overlapping layer between the wall location $y = 0$ and the interface height $y = h_{wm}$

$$\frac{d}{dy} \left[(\mu + \mu_{t,wm}) \frac{dU_{||}}{dy} \right] = 0 \quad (1)$$

$$\frac{d}{dy} \left[(\mu + \mu_{t,wm}) U_{||} \frac{dT}{dy} + c_p \left(\frac{\mu}{Pr} + \frac{\mu_{t,wm}}{Pr_{t,wm}} \right) \frac{dT}{dy} \right] = 0 \quad (2)$$

where $U_{||}$ and T are the wall-parallel velocity and the temperature. According to the equations, solving the equilibrium wall model only needs the wall-normal grid connectivity. These equations are derived from the conservation equations for streamwise momentum and total energy with use of the standard approximations in equilibrium-boundary-layer flow. The pressure is assumed to be wall-normal independent and equal to the outer-layer LES solution at the interface height $y = h_{wm}$. The mixing-length eddy-viscosity model $\mu_{t,wm} = \kappa \rho y \sqrt{\tau_w / \rho} D$ with near-wall damping $D = [1 - \exp(-y^+ / A^+)]^2$ is used to determine the $\mu_{t,wm}$ in the inner-layer wall model. $\sqrt{\tau_w / \rho}$ is the velocity scale in a boundary layer with the local instantaneous density and wall stress, y^+ is the distance from the wall in wall units and $A^+ = 17$. The von Karman constant $\kappa = 0.41$ and turbulent Prandtl number $Pr_{t,wm} = 0.9$. In this study, $\mu_{t,wm}$ is computed from $x/c = 0.07$ on both suction and pressure sides of the airfoil to model the forced laminar-turbulent transition according to the experiment.

From our previous studies, it is possible to accurately resolve the outer layer turbulence by resolving the boundary layer at more than 20 mesh points. Since the required mesh resolution depends on the local boundary layer thickness, it is necessary to place meshes of smaller size near the leading edge where the boundary layer becomes thinner. Then, the computational grid is smoothly stretched as the boundary layer develops. A C-type structured mesh is generated. Outer boundary is located $80c$ away from the airfoil in η direction. The spanwise length is set to $0.065c$ which is the maximum separation width at $x/c = 0.75$. Mesh was generated to satisfy $\delta/\Delta x = \delta/\Delta y \geq 25$ in each chord position. Points are $\xi \times \eta \times \zeta = 4603 \times 169 \times 565$. The mesh resolution is $\Delta\xi^+ = \Delta\eta^+ = \Delta\zeta^+ \approx 9.6$ and $h_{wm}^+ \approx 60$ based on the wall unit at $x/c = 0.2$. Due to the large $\Delta\eta^+$, the time-step size can be increased by one-order of magnitude compared to the traditional wall-resolved LES. The nondimensionalized time step $\Delta t = 1.5 \times 10^{-5}$ based on the chord length and the freestream speed of sound. This time step results in the maximum Courant-Friedrichs-Levy number of 0.4.

RESULTS

The flow conditions of buffet condition are $Re_c = 3.0 \times 10^6$, $\alpha = 3.5deg$, and $M_\infty = 0.73$. To investigate the capability of the buffet onset prediction, the result of RANS computation with Baldwin-Lomax turbulence model (Baldwin and Lomax, 1978) at buffet condition and the WMLES computation at non-buffet condition ($Re_c = 3.0 \times 10^6$, $\alpha = 3.5deg$, and $M_\infty = 0.715$) are also computed. Figure 1(a) shows the averaged pressure coefficient $C_p = 2(p - p_\infty)/\rho_\infty u_\infty^2$. In the RANS computation, the shock wave does not oscillates, and typical C_p distribution is obtained. Zonal DES can predict the shock oscillation by tuning the size of RANS region (Deck, 2005). However, the region in which the shock wave oscillates is estimated more upstream than experiment. Furthermore, the separation near the trailing edge is predicted larger. At non-buffet condition ($M_\infty = 0.715$) of the WMLES computation, the shock wave does not move as well as RANS computation. WMLES at the buffet condition ($M_\infty = 0.73$) can predict the shock oscillation and C_p slope which is observed at the oscillation region in the experiment is also obtained. In addition, the reattachment behind the shock wave and the small separation near the trailing edge are precisely predicted. The region in which the shock wave moves has some difference between the experiment (Jacquin et al., 2009) and the WMLES. Figure 1(b) shows the surface pressure fluctuation $\sqrt{p'p'}/p_\infty$. Zonal DES computation estimates the larger pressure fluctuation than experiment near the shock wave and the trailing edge. WMLES provides small fluctuation at non-buffet condition and large fluctuation at buffet condition. In buffet condition, the shock wave moves at more downstream region in the WMLES. Therefore, it can be considered that the flow is accelerated and the shock wave become stronger than that in the experiment. As a results, the pressure fluctuation becomes larger.

Figure 2(a) shows the streamwise velocity $u^+ = \bar{u}/\sqrt{\tau_w/\rho}$ compared with log-law $(\ln(y^+)/0.41 + 5.2)$ at the completely developed attached turbulent boundary layer position before the interaction with the shock wave ($x/c = 0.3$). The velocity distribution satisfies the log-law. Figure 2(b) shows the Reynolds shear stress $-\bar{\rho}u'v'/\tau_w$ compared with RANS results at the same position. Turbulent boundary layer is fully developed upstream of the shock wave.

Figure 3 shows the trace of the shock wave position in the WMLES computation. In buffet condition, the shock wave moves from $x/c = 0.48$ to $x/c = 0.6$ at $St_s = f_s c/M_\infty \approx 0.065$. This Strouhal number is 70.1Hz at $c = 230mm$ which nearly equals to the buffet frequency obtained from experiment. On the other hand, in non-buffet condition, it turns out that the shock wave oscillates in a very

narrow region. This phenomenon is also observed in experiments.

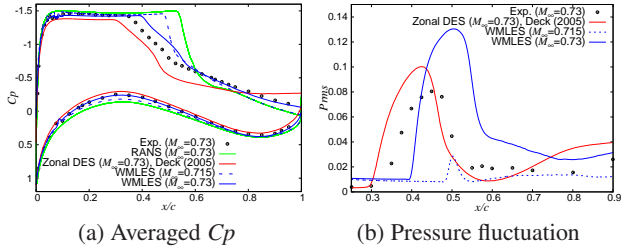


Figure 1. Averaged C_p and pressure fluctuation along the airfoil compared to the experiment and the Zonal DES.

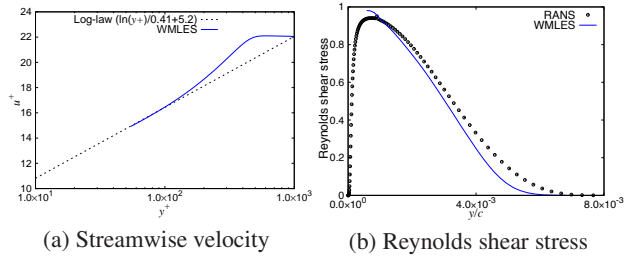


Figure 2. Streamwise velocity and Reynolds shear stress at the completely developed attached turbulent boundary layer position ($x/c = 0.3$).

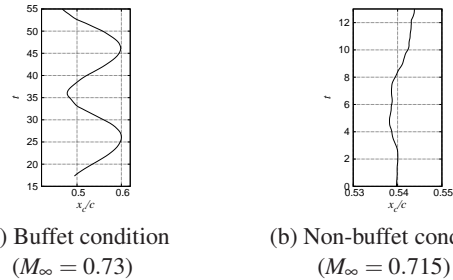


Figure 3. Shock wave position $0.2c$ away from the wall.

BUFFET MECHANISMS

In this section, the self-sustained oscillation mechanisms are investigated. In the majority of previous studies, it is considered that the shock wave is oscillated by acoustic waves which are generated from the trailing edge, and the sources of acoustic waves are vortical structures which convect in the separated shear layer (Lee, 2001). We will verify these theories by analyzing the buffet and non-buffet flow fields.

There are some physical phenomena in the buffet flow field, i.e., the shock wave, acoustic waves and the turbulent boundary layer. First, we will identify the frequency band of these phenomena by checking the frequency weighted power spectrum density (FWPSD) distribution of the wall surface pressure p/p_∞ . FWPSD highlights the frequencies which contribute most to the pressure fluctuation.

ation. FWPSD is obtained from the equation as below.

$$FWPSD(f) = \frac{f \cdot PSD(f)}{\int_0^\infty f \cdot PSD(f) df} \quad (3)$$

where $PSD(f)$ is PSD function.

Figure 4 shows FWPSD distribution of buffet and non-buffet conditions. In buffet condition, the spectrum of a low frequency band is the largest. The fluctuation of this low frequency band is due to the shock wave movement, and it is observed that the shock wave movement affects the entire flow field around the airfoil. Near the trailing edge, it is considered that the separated shear layer is largely flapped due to the shock wave movement. From trip position to the shock wave, the contribution of the low frequency fluctuation is small. This is because that the turbulent boundary layer develops from trip position and the contribution of the fluctuation due to the shock wave movement becomes relatively small. In the higher frequency band, peaks are observed near the trailing edge around $St \approx 3$. Since this is also shown in non-buffet condition, it is considered to be irrelevant to shock wave movement. Additionally, there is a spectrum seen from the shock wave position with slightly higher frequency than $St \approx 3$. This fluctuation is considered to be the separation of the turbulent boundary layer by the shock wave and the accompanying vortex shedding. These vortices are considered to be the sources of the trailing edge noise.

In non-buffet condition, fluctuation of low frequency band is small and fluctuation near the trailing edge is hardly observed because the shock wave movement is small.

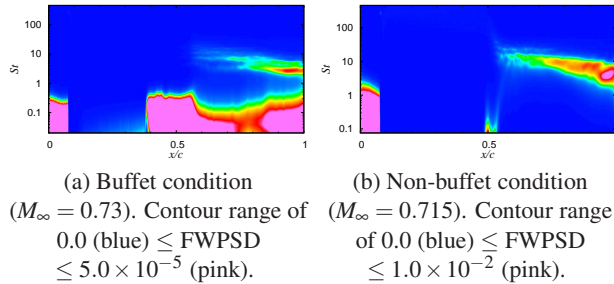


Figure 4. FWPSD distribution of the wall surface pressure.

From the FWPSD of the pressure fluctuation, it is clear that there are mainly two fluctuations which are low frequency fluctuation due to the shock wave movement and high frequency fluctuation which is vortex shedding in the separated turbulent boundary layer. Since these fluctuations have completely different amplitudes, the characteristics of these low and high frequency bands are analyzed separately. For this purpose, the phase average operation is performed to separate the low and high frequency components. The fluctuation is decomposed as $u(x, t) = \bar{u}(x) + \tilde{u}(x, t) + u'(x, t)$. $\bar{u}(x)$ is the total ensemble average. $\tilde{u}(x, t)$ is low frequency periodic component. $u'(x, t)$ is the high frequency random component. By averaging the physical fluctuation at each phase of periodic component, low and high frequency components can be separated. Additionally, by subtracting the total ensemble average component $\bar{u}(x)$ from the phase average component $\bar{u}(x) + \tilde{u}(x, t)$, low frequency component is separated from the phase average component. It is assumed that there are N sample data, the sample data at each coordinate x and i th time step is $u(x, t_i)$, and N_p sample data constitutes the each phase. The phase average component and total ensemble component are

computed as bellow,

$$\bar{u}(x) + \tilde{u}(x, t) = \langle u(x, t_i) \rangle = \frac{1}{N_p} \sum_{j=-N_p/2}^{N_p/2} u(x, t_i + \Delta t \cdot j) \quad (4)$$

$$\bar{u}(x) = \overline{u(x, t_i)} = \frac{1}{N} \sum_{i=1}^N u(x, t_j) \quad (5)$$

$\langle \rangle$ denotes the phase average operation. From these components, $\tilde{u}(x, t)$ and $u'(x, t)$ at each time t are computed as $\tilde{u}(x, t) = \langle u(x, t_i) \rangle - \overline{u(x, t_i)}$ and $u'(x, t) = u(x, t_i) - \langle u(x, t_i) \rangle$.

The periodic component of buffet flow is shock wave movement. Therefore, N should be set from the time steps which constitute the shock wave movement. N_p can be set arbitrarily and is associated with the frequency which separates the low and high frequency components. The truncation frequency is assumed $St_t = c/(\Delta t \cdot N_p)/u_\infty$. By phase average operation, random component of the frequency higher than this frequency is damped. $St_t \approx 1$ is appropriate from Fig. 4. In this study, flow data is sampled every 100 time step. Therefore, N_p is set to 1,000 and $St_t = c/(100 \cdot \Delta t \cdot N_p)/u_\infty \approx 0.9$.

Figures 5 and 6 show the periodic and random components of pressure fluctuations. The shock wave is moving downstream at $t = 20.2$ and upstream at $t = 32.2$. In Fig. 5, the pressure near the trailing edge is relatively high at $t = 20.2$. When the shock wave reaches the most downstream, the low pressure part accompanying the separation of the turbulent boundary layer is generated from the foot of the shock wave. The low pressure part becomes larger as it convects to the trailing edge. When the low pressure part reaches the trailing edge, it seems to propagate upstream from the pressure side of the airfoil. From these results, it can be considered that when the shock wave moves upstream, a large vortical structure is generated accompanying the separation of the turbulent boundary layer in low frequency band. Acoustic waves propagating upstream will be generated from the theory of trailing edge noise. In Fig. 6, pressure fluctuations in the shear layer and acoustic waves generated from the trailing edge can be observed in any of the time series. When the shock wave moves downstream, the shear layer attaches and the fluctuation in the shear layer is weak. On the other hand, when the shock wave moves upstream, the fluctuation becomes strong due to the large separation of the shear layer, and the acoustic waves generated from the trailing edge also becomes strong. At $t = 20.2$, the acoustic waves propagate to the upstream part of the shock wave through the subsonic region above the shock wave. In addition, the acoustic waves also propagate to the upstream of the shock wave through the pressure side of the airfoil. It is considered that the pressure at the upstream of the shock wave is affected by these acoustic waves. In fact, the pressure at the upstream of the shock wave fluctuates at low frequency in Fig. 5.

It is obvious that the pressure fluctuations in Fig. 6 are small-scale vortical structures generated in the separated shear layer. However, it is not clear that the low pressure part seen in Fig. 5 is driven from the vortical structures. Therefore, it is confirmed whether the vortical structures are included in the periodic component and the relation with the flow field is investigated by checking the vorticity magnitude and the streamwise velocity of the periodic component. Figures 7 and 8 show the periodic component of vorticity magnitude $|\nabla \times \tilde{u}|$ and the streamwise velocity \tilde{u} . In buffet condition, strong vorticity appears constantly at the position of the shear layer compared with non-buffet condition. In addition, a large

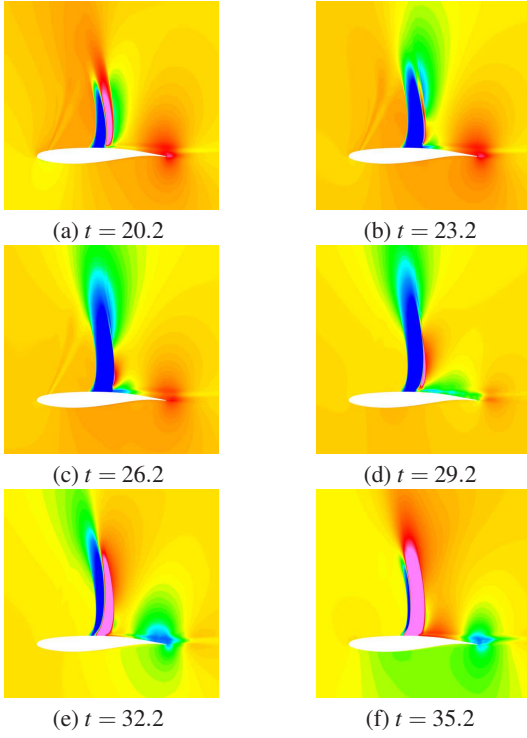


Figure 5. Periodic pressure fluctuations at $M_\infty=0.73$. Contour range of -0.07 (blue) $\leq \tilde{p}/p_\infty \leq 0.07$ (pink).

vortical structure occurs especially when the shock wave moves upstream. On the other hand, only small vorticity can be observed in non-buffet condition. Therefore, it is confirmed that the large-scale vortical structure generates in the separated shear layer with low frequency band only in buffet condition. From Fig. 8, when the shock wave moves upstream, the periodic component of the streamwise velocity is negative, and it is considered that the flow velocity becomes slower or adverse flow occurs. On the other hand, there is small periodic component in non-buffet condition. From the results, when the shock wave moves upstream, the large-scale vortical structure with low frequency band is generated due to separation of the shear layer in buffet condition. At the same time, the flow velocity becomes slower, and this vortical structure advects with low velocity.

Next, we compute the space-time correlation of the pressure fluctuation in order to identify the characteristics of the dominant phenomena in the periodic component. In this research, direction and velocity of advecting vortices and propagating acoustic waves are confirmed. Space-time correlation of pressure fluctuation is computed as bellow,

$$R_{nm}(x_m, \tau) = \frac{\overline{p(x_n, t)p(x_m, t + \tau)}}{\sqrt{\overline{p(x_n, t)^2}}\sqrt{\overline{p(x_m, t)^2}}} \quad (6)$$

where x_n is the reference position of the correlation from the leading edge. x_m is the position to compute the correlation with the reference position. τ is the time lag to compute the correlation with the reference time. Correlations on airfoil surface and $0.53c$ above the airfoil are computed because the vortices in the shear layer should be dominant on surface, and acoustic waves generated from the trailing edge should be dominant out of the shear layer. Since the contribution of the random component is the maximum around $x/c = 0.95$ from Fig. 4, the reference position x_n/c is set to 0.95. x_n/c is set to 0.85 at $0.53c$ away from the wall because there

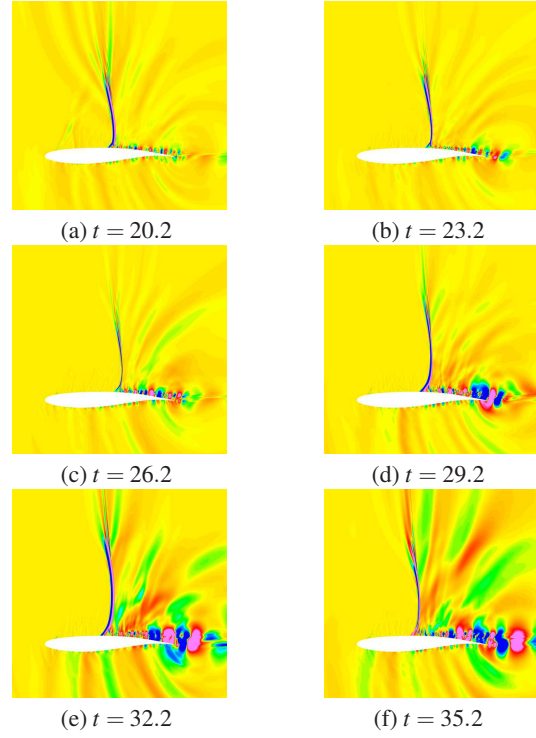


Figure 6. Random pressure fluctuations at $M_\infty=0.73$. Contour range of -0.015 (blue) $\leq p'/p_\infty \leq 0.015$ (pink).

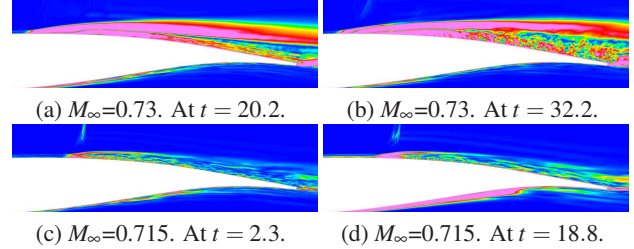


Figure 7. Periodic components of vorticity magnitude. Contour range of 0.0 (blue) $\leq |\nabla \times (\tilde{u}/u_\infty)| \leq 10.0$ (pink).

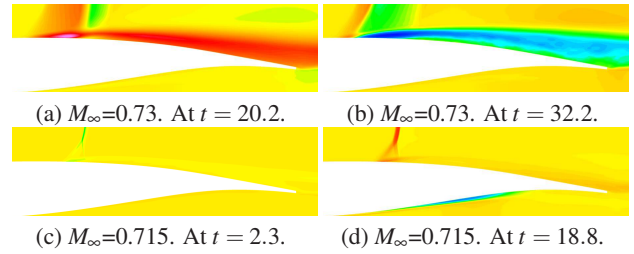


Figure 8. Periodic components of streamwise velocity. Contour range of -0.68 (blue) $\leq \tilde{u}/u_\infty \leq 1.0$ (pink).

are peaks near $x/c = 0.85$ in FWPSD distribution at $0.53c$ away from the wall.

Figure 9 shows the correlations of periodic component. In buffet condition, it can be seen that correlation changes at the same cycle as the period of the shock wave movement, and the peak of the correlation moves downstream. It means that the shock wave movement and the advection to downstream are dominant in low frequency band. This advecting flow includes the vortices generated in the separated shear layer. In non-buffet condition, large-scale

correlation is not observed because the range of the shock wave movement is small. By tracing the peak values of the correlation at each chord position, the velocity of dominant phenomena can be estimated. The velocities of $0.14u_\infty$ in buffet condition and $0.50u_\infty$ in non-buffet condition are obtained. From the results, it is considered that the shear layer separates due to movement of shock wave, and reverse flow occurs in buffet condition. Therefore, the advection velocity of the low frequency vortical structure becomes slower than $0.50u_\infty$, and the velocity of $0.14u_\infty$ is observed.

At the outside the separated shear layer, the same correlation change as the cycle of shock wave movement is also observed in buffet condition. Near the shock wave, there is a correlation that moves to the upstream side of the shock wave. Velocity of the correlation are $0.135u_\infty$ which is much smaller than the value considered as the velocity of acoustic wave propagating in the flow field. Therefore, it seems that other phenomena which is associated with the shock wave movement appears. In non-buffet condition, the inverse correlation at the front and back of the shock wave is observed. In addition, the velocity at the reference position is $-0.61u_\infty$. This velocity is considered to be the propagation velocity of low frequency acoustic waves because the shock wave hardly oscillates. From the results, it is thought that low frequency trailing edge noise occurs when the large-scale vortical structures passes through the trailing edge.

It is considered that the trailing edge noise fluctuates the pressure before the shock wave through the upper part of the shock wave and the pressure side of the airfoil. However, the influence of the acoustic waves cannot be identified in this research. If the shock wave is oscillated by these acoustic waves, it can be considered that the buffet frequency is estimated from these characteristic velocities of vortical structures and acoustic waves. In addition, low frequency acoustic waves are thought to be the cause of buffet phenomenon because the buffet frequency is contained in the low frequency band.

The velocity of the large-scale vortical structures is considered as $0.14u_\infty$. We will estimate the velocity of low frequency acoustic waves from the result of buffet condition. However, it cannot be identified because the shock wave fluctuation is much larger than that of acoustic waves. Therefore, in this study, the velocity is estimated from the correlation of non-buffet condition which is $-0.61u_\infty$. This velocity is similar to that of the random component in buffet condition. Therefore, this velocity is considered to be the velocity of acoustic waves. The buffet frequency can be estimated by the following equation.

$$St_s = \left(\frac{c - x_{s,ave}}{a_p} + \frac{c - x_{s,ave}}{|a_u|} \right)^{-1} \quad (7)$$

where St_s is the buffet frequency, $x_{s,ave}$ is the mean shock position which is $0.5c$ in this research, a_p and a_u are velocities of vortical structures and acoustic waves. From the results, the buffet frequency is estimated as 0.23 which is one order of magnitude higher than the buffet frequency estimated from the trajectory of the shock wave movement. From the above results, it can be confirmed that there are the large-scale vortical structures constituting the acoustic feedbacks loop model and low frequency acoustic waves generated by the vortical structures. However, it cannot be identified how much acoustic waves affect the pressure forward and backward of the shock wave. In addition, the buffet frequency estimated from the advection velocity of the vortical structures and the propagation velocity of the acoustic waves is much different from the results obtained from the trajectory of the shock wave.

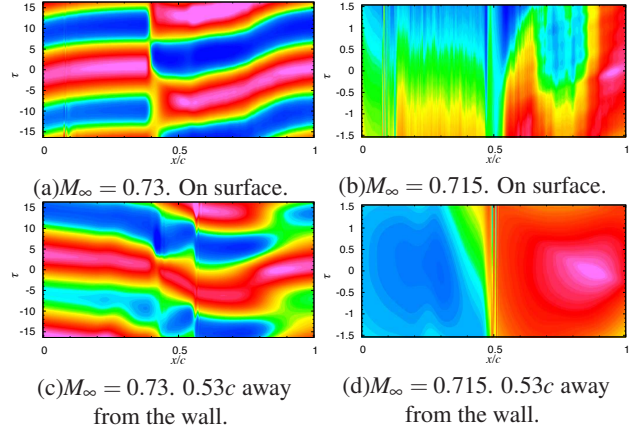


Figure 9. Space-time correlation of periodic component of pressure fluctuation. Contour range of -1.0 (blue) $\leq R_{nm} \leq 1.0$ (pink).

PROPOSED MODEL

We propose a new self-sustained oscillation model in this section. In the acoustic feedback loop model, the pressure fluctuation observed in the periodic component is considered to be the fluctuation of acoustic waves (Fig. 5). However, this low frequency fluctuation also includes fluctuation due to separation of the shear layer. In the proposed model, we consider that the pressure fluctuation due to separation of the shear layer drives the shock wave. Across the shock wave, the Rankine-Hugoniot equation is described in Eqs. 8 and 9.

$$\frac{p_2}{p_1} = 1 + \frac{2\gamma}{\gamma+1} (M_1^2 - 1) \quad (8)$$

$$M_2 = \sqrt{\frac{1 + [(\gamma-1)/2]M_1^2}{\gamma M_1^2 - (\gamma-1)/2}} \quad (9)$$

where p_1 and p_2 are pressures forward and backward of the shock wave. M_1 and M_2 are the Mach number forward and backward of the shock wave. These equations mean that the effective Mach number of the shock wave is defined by the pressure ratio. When the pressure ratio changes, the shock wave should become weak or strong and moves forward or backward to balance the equations. Variation in pressure ratio is caused by the shock induced separation of the boundary layer. Figure 10 express the proposed model. When the shock wave is at the most downstream, relatively large separation occurs and the flow area decreases as shown in Fig. 5. Therefore, the flow velocity increases and the pressure behind the shock wave decreases. As a result, pressure ratio decreases and the shock wave should weaken. Then, the shock wave moves upstream to balance the Eqs. 8 and 9. On the other hand, when the shock wave is at the most upstream, the separation disappears and the flow area increases. Therefore, the flow velocity decreases and the pressure behind the shock wave increases. As a result, pressure ratio increases, and the shock wave should become strong and moves downstream.

Figure 11 shows the time history of the shock wave position, span averaged pressure and local Mach number near the trailing edge and the separation size. The shock wave position is defined by the position with maximum pressure ratio at $0.2c$ away from the wall. Pressure and local Mach number are sampled at the point of

$x/c = 0.9$ and $z/c = 0.19$ from the leading edge. The shear flow thickness is defined by the thickness from the wall to the position where Mach number is 0.5. In Fig. 11, due to the movement of the shock wave, values fluctuate largely. When the shock wave is at the most downstream, the shear layer thickness begins to increase. As a result, the pressure decreases and the Mach number increases. When the shock wave is at the most upstream, the shear layer thickness begins to decrease. As a result, the pressure increases and the Mach number decreases. From the results, the proposed model is investigated from the obtained flow field.

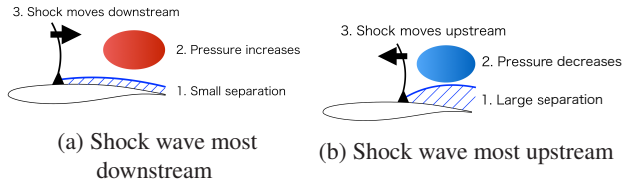


Figure 10. Proposed model.

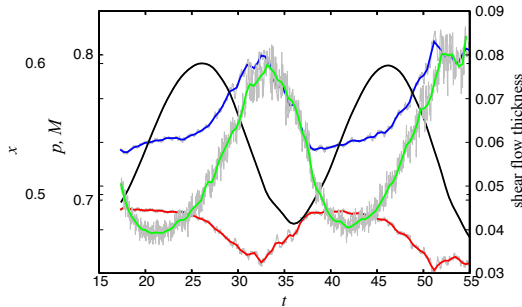


Figure 11. Physical quantities fluctuation during shock wave oscillation. Grey lines are the raw data. Black and colored lines are the interpolated data by cubic spline. Black line is shock wave position $0.2c$ away from the wall. Red line is pressure. Blue line is local Mach number. Green line is shear flow thickness.

CONCLUSIONS

The transonic buffet phenomena over the OAT15A supercritical airfoil at high Reynolds number was computed by the WMLES. By using the WMLES, the buffet onset was successfully predicted. Pressure distributions showed the WMLES could simulate the small separation near the trailing edge with the buffet phenomena. According to the trace of the shock wave position, it was confirmed that the shock wave oscillated at the same frequency as that of the experiment. The self-sustained oscillation mechanisms of buffet phenomena were investigated from the obtained results. As a result, it was confirmed that there are dominant phenomena in low and high frequency band which are the shock wave movement and the vortex shedding from the separated shear layer. By using the phase average operation, large-scale vortical structures with low frequency in the separated shear layer and the acoustic waves generated from the trailing edge were identified. It was also confirmed that acoustic waves propagate upstream of the shock wave through the upper and lower side of the airfoil. However, Lee's acoustic

feedback loop model was unable to predict the buffet frequency. On the other hand, we proposed the new self-sustained oscillation model. In the proposed model, the shock wave oscillation depends on the pressure ratio forward and backward of the shock wave, and the pressure variation is caused by the shock induced separation of the shear layer. The possibility of the proposed model was confirmed from the obtained results. The remaining problem is determining the buffet frequency in the proposed model.

ACKNOWLEDGEMENTS

This work was supported in part by MEXT as a social and scientific priority issue (Development of Innovative Design and Production Processes that Lead the Way for the Manufacturing Industry in the Near Future) to be tackled by using post-K computer. A part of this research used computational resources of the K computer provided by the RIKEN Advanced Institute for Computational Science (Project ID:hp150254, hp160205, hp170267)

REFERENCES

- Choi H. & Moin P. 2012 Grid-point requirements for large eddy simulation: Chapman's estimates revisited. *Physics of Fluids* **24**, 011702-1 - 011702-5.
- Larsson, J., Kawai, S., Bodart, J. & Bermejo-moreno, I. 2016 Large eddy simulation with modeled wall-stress: recent progress and future directions *Mechanical Engineering Reviews* **3**, 15-00418.
- Kawai, S. & Larsson, J. 2012 Wall-modeling in large eddy simulation: length scales, grid resolution and accuracy *Physics of Fluids* **24**, 015105-1 - 015105-10.
- Kawai, S. & Larsson, J. 2013 Dynamic non-equilibrium wall-modeling for large eddy simulation at high Reynolds numbers *Physics of Fluids* **25**, 015105-1 - 015105-21.
- Kawai, S. & Asada, K. 2013 Wall-modeled large-eddy simulation of high Reynolds number flow around an airfoil near stall condition *Computers and Fluids* **85**, 105-113.
- Deck, S. 2005 Numerical simulation of transonic buffet over a supercritical airfoil *AIAA Journal* **43**, 1556-1566.
- Hartmann, A., Feldhusen, A. & Schroder, W. 2013 On the interaction of shock waves and sound waves in transonic buffet flow *Physics of Fluids* **25**, 026101-1 - 026101-17.
- Lele, S. K. 1992 Compact finite difference schemes with spectral-like resolution *Journal of Computational Physics* **103**, 16-42.
- Gaitonde, D. V. & Visbal, M. R. 2000 Pade-type higher-order boundary filters for the Navier-Stokes equations *AIAA Journal* **38**, 2103-2112.
- Gottlieb, S. & Shu, C. W. 1998 Total variation diminishing Runge-Kutta scheme *Mathematics of Computation* **67**, 73-85.
- Kawai, S., Shankar, S. K. & Lele, S. K. 2010 Assessment of localized artificial diffusivity scheme for large-eddy simulation of compressible turbulent flows *Journal of Computational Physics* **229**, 1739-1762.
- Lenormand, E., Sagaut, P. & Phuoc, T. L. 2000 Large eddy simulation of subsonic and supersonic channel flow at moderate Reynolds number *International Journal for Numerical Methods in Fluids* **32**, 369-406.
- Baldwin, S. B. & Lomax, H. 1978 Thin layer approximation and algebraic model for separated turbulent flows AIAA Paper 78-257.
- Jacquin, L., Molton, P., Deck, S. Maury, B. & Soulevant, D. 2009 Experimental study of shock oscillation over a transonic supercritical profile *AIAA Journal* **47**, 1985-1994.
- Lee, B. H. K. 2001 Self-sustained shock oscillations on airfoils at transonic speeds *Progress in Aerospace Sciences* **37**, 147-196.